Structural Transformations in Ferroelectrics Discovered by Raman Spectroscopy

Kai Jiang, Liping Xu, Jinzhong Zhang,
Zhigao Hu and Junhao Chu

Additional information is available at the end of the chapter

Abstract

Ferroelectrics systems are of great interest from the fundamental as well as applications points, such as ferroelectric random access memories, electro-optic switches and a number of electro-optic devices. Curie temperature (T_C) is one of the important parameters of ferroelectrics for high-temperature applications. Particularly, the optical modes, which are associated with the ferroelectric to paraelectric phase transition, are of great interest. Structural transformations that alter the crystal symmetry often have a significant effect on the Raman spectroscopy. This chapter systematically studies the type ferroelectric oxides and rare earth element doped ferroelectric materials such as $PbTiO_3$-$Bi(Mg_{0.5}Ti_{0.5})O_3$ (PT-BMT), $Sr_xBa_{1-x}Nb_2O_6$ (SBN), $Pb_{1-1.5x}La_xZr_{0.42}Sn_{0.4}Ti_{0.18}O_3$ (PLZST), $Bi_{1-x}La_xFe_{1-y}Ti_yO_3$ (BLFT) and $(K_{0.5}Na_{0.5})NbO_3$-$0.05LiNbO_3$ (KNN-LN) and so on synthesis of single crystal/ceramic and optical phonon vibration modes and the improvement of the Curie temperature characteristic using spectrometry measurements. The T_C, distortion degree, and phase structure of the ferroelectric materials have been investigated by temperature-dependent Raman spectroscopy. Meanwhile, the important physical parameters exhibited a strong dependence on dopants resulting in structural modifications and performance promotion.

Keywords: ferroelectrics, Raman spectra, vibration modes, phase transitions, Curie temperature

1. Introduction

As we know, ferroelectric ceramics were first found in barium titanate ceramic with the ferroelectricity in the 1940s [1]. Since that time, the ferroelectric material with high resistivity, good fatigue resistance characteristic and high dielectric constant, pyroelectric detector, uncooled infrared detectors, uncooled infrared focal plane arrays and ferroelectric memory, and other

fields has great application prospect [2–5]. In recent years, complex mixed-ion ferroelectric materials have been extensively investigated in order to achieve optimum properties as well as to understand the underlying factors for property tweaking [6–9]. Therefore, the ferroelectric materials are considered to be one of the most practical materials in the future.

The ABO_3 ferroelectric materials have achieved wide usage owing to their superior electromechanical properties (**Scheme 1** shows the typical structure). Investigations of bulk ferroelectric materials have demonstrated good macroscopic homogeneity of their properties and clear ferroelectric behavior [2]. However, the development of knowledge about ferroelectric behavior at the submicrometer level is relatively slow. It has been found that the structural and chemical factors such as grain size, strain, stoichiometric and compositional homogeneity and phase structure, have great effect on optimization and reproducibility of the property coefficients in ferroelectric materials [10–12]. Therefore, a further investigation should be necessary in order to illustrate the physical mechanism in these ferroelectrics.

It is important to remember that the experimentally obtained parameters depend primarily on the spatial magnitude and time-scale of the measured physical phenomena, especially for studying the structure–property correlations in these materials. Raman spectroscopy is a sensitive technique for investigating the structure modifications and lattice vibration modes, which can give the information on the changes of lattice vibrations and the occupying positions of doping ions. Structural changes that alter the crystal symmetry often have a significant effect on the Raman spectrum. In addition, spatially resolved Raman spectroscopy can be used to probe the chemical homogeneity at sub-micrometer levels. This chapter provides a review of systematic Raman scattering study on the phase transition behavior in perovskites, tungsten bronze, Aurivillius layered, multiferroics and lead-free bulk materials. The effect of A- and B-site substitutions on the Raman spectra and phase transition behavior of these materials have been studied in detail. This chapter is arranged in the following way. In Section 1, research background; In Section 2, detailed growths of the ferroelectric materials and Raman experiment; In Section 3, results of Raman spectra in $PbTiO_3$-$Bi(Mg_{0.5}Ti_{0.5})O_3$ (PT-BMT), $Sr_xBa_{1-x}Nb_2O_6$ (SBN), $Pb_{1-1.5x}La_xZr_{0.42}Sn_{0.4}Ti_{0.18}O_3$ (PLZST), $Bi_{1-x}La_xFe_{1-y}Ti_yO_3$ (BLFT) and $(K_{0.5}Na_{0.5})NbO_3$-0.05LiNbO_3$ (KNN-LN); at last, the main results and remarks are summarized.
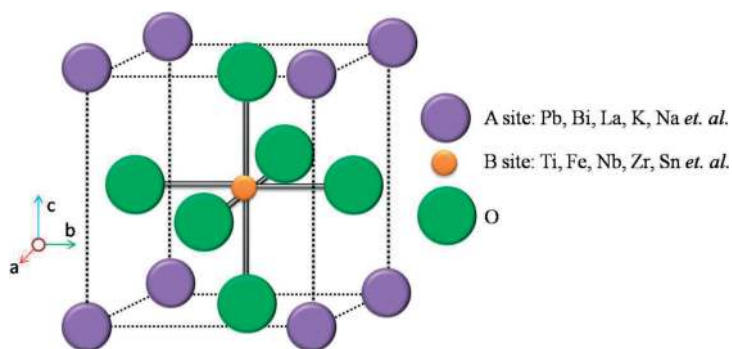
Scheme 1. Schematic representation of the typical ABO_3 ferroelectric structure.

2. Experiment details

2.1. Fabrication of ferroelectric materials

The ferroelectric single crystals have been grown by a high temperature solution method (flux method) [13, 14]. High-purity powders were selected as starting materials. The raw material powders were stoichiometrically weighed, mixed by milling with zirconia media in the ethanol as a solvent. After drying. The powders were calcined at a certain temperature for hours to form the desired perovskite phase. Details of the fabrication process for the single crystals can be found elsewhere [13].

The bulk ceramics were fabricated by a conventional solid state reaction sintering, using the appropriate amount of reagent grade raw materials [15, 16]. The samples were sintered at different temperature for several hours in air atmosphere, and then remilled for several hours to reduce the particle size for sintering. The calcined powders were added with 8 wt.% polyvinyl alcohol (PVA) as a binder. Before Raman measurements, the ceramics with the diameter of 15 mm and the thickness of 1 mm were rigorously single-side polished and cleaned in pure ethanol with an ultrasonic bath and rinsed several times by deionized water.

2.2. Raman experiment details

Raman scattering experiments were carried out using a Jobin-Yvon LabRAM HR 800 UV micro-Raman spectrometer, excited by 632.8 nm He-Ne laser or 488 nm Ar laser and recorded in the frequency range of 10–1000 cm^{-1} with a spectral resolution of 0.5 cm^{-1}. For the different temperature Raman spectra, we choose a $50\times$ microscope with a long working distance of 18 mm. The spectrometer grating can be choosed by 600, 1800 or 2400 grooves/mm grating which is depending on the different excitation wavelength. In order to learn more about the variation trend of vibration modes, all of the experimental spectra were fitted with independent damped harmonic oscillators. The polarized Raman spectra were recorded in back-scattering geometry in parallel $<x|zx|y>$ (VH) and perpendicular $<x|zz|y>$ (VV) polarization configurations. Temperature dependent Raman spectra were collected with a THMSE 600 heating/cooling stage (Linkam Scientific Instruments) in the temperature range from 77 to 800 K with a resolution of 0.1 K.

3. Results and discussion

3.1. PbTiO$_3$-based single crystals

PbTiO$_3$ (PT)-based perovskite compounds are important multifunctional materials, which have been investigated in the last half century due to their controllable physical properties. Most recently, the research hotspot for PbTiO$_3$-BiMeO$_3$ ferroelectrics have stimulated much interest [14]. A range of compelling information on thermal expansion behavior and lattice dynamics of novel ferroelectric perovskite-type 0.62PbTiO$_3$-0.38Bi(Mg$_{0.5}$Ti$_{0.5}$)O$_3$ (PT-BMT) single crystal has been revealed by means of temperature-dependent X-ray diffraction and polarized Raman scattering. **Figure 1** shows the polarized Raman spectra of 0.62PT-0.38BMT single
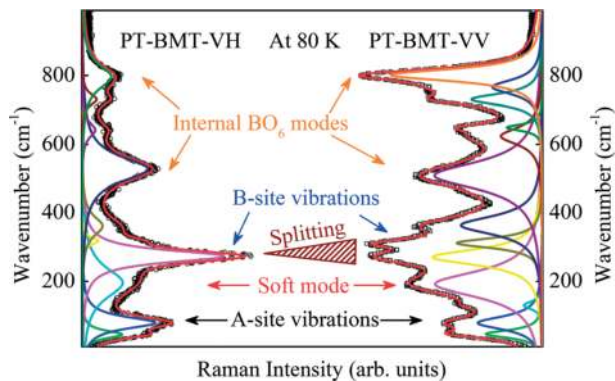
Figure 1. The polarized VH and VV Raman spectra of 0.62PT-0.38BMT single crystal at 80 K. The peak assignment is based on the individual vibration mode, which is fitted by Lorentz function (Figure reproduced with permission from [14]. Copyright 2016, Royal Society of Chemistry).

crystal at representative temperature of 80 K. It can be found that the Raman spectra is consistent with previous reports of the tetragonal crystal structure. Comparing to the theoretical calculations and experimental results, three main regions with different kinds of vibration in the lattice can be distinguished: (1) Low frequency below 150 cm^{-1}, which can be associated with vibrations of the perovskite A-site, involving Pb and Bi ions. (2) Frequency range 150–450 cm^{-1}, which is related to the Ti-O/Mg-O stretching vibrations. (3) High frequency bands above 450 cm^{-1} have all been associated with BO$_6$ vibrations, namely the breathing and stretching modes of the oxygen octahedra. The Raman spectra suggest a certain degree of local B-site chemical order for the 0.62PT-0.38BMT single crystal with A-site and B-site simultaneously doping.

In order to understand the relationship between negative thermal expansion (NTE) and lattice dynamic behavior for the 0.62PT-0.38BMT crystal, **Figure 2** presents the polarized Raman spectra in different temperature point from 80 to 850 K. It can be found that the peak position and intensity of the polarized Raman phonon modes have a decreasing trend with increasing temperature, while the broadening of the Raman modes is observed, which is consist with the other ferroelectrics [17]. It should be pointed that around the temperature range of 600–700 K, the lowest phonon modes occurs (marked by the dashed rectangles). In XRD results, we can also found the similar anomalies range (different coefficient of thermal expansion values in **Figure 3**). Thus, there are some minor structural changes in the tetragonal PT-BMT crystal, which is corresponding to the change of the Raman phonon modes above 700 K. This phenomenon is the result of interaction by spontaneous volume ferroelectrostriction mechanism and the dynamics of the polar nanoregions (PNRs).

Figure 3 shows the different temperature Raman spectra with different changing trend. As we know, an abnormal phonon softening upon heating can be detected by high resolution Raman spectra if there is any phase transition change. From the 0.62PT-0.38BMT Raman spectra, one clear anomaly is observed at about 670 K, which is quite different from the phase transition temperature. We found the Curie temperature of this single crystal is located at about 800 K through the XRD pattern and dielectric permittivity experiment. The PNRs can play an important role in
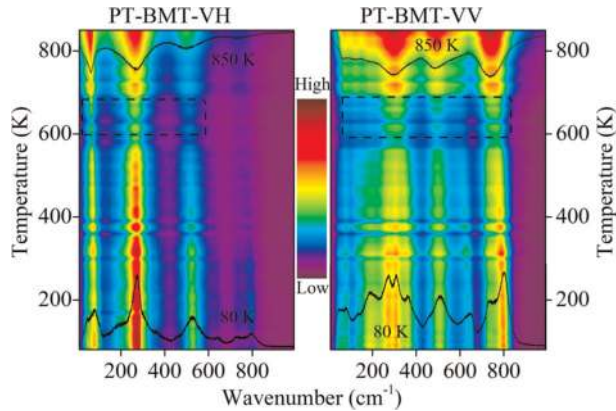
Figure 2. Temperature evolution of Raman intensities for 0.62PT-0.38BMT single crystal. The dashed rectangles mark the temperature ranges of the most pronounced changes (Figure reproduced with permission from [14]. Copyright 2016, Royal Society of Chemistry).

lead-based ferroelectric materials. Note that the physical properties of the single crystal have some linear changes near phase transition, for example the refractive index n, lattice parameters, and unit cell volume V. Thus, the abnormal increasing for the soft mode indicates some structure changes from the crystal Raman spectra. In the whole temperature range, two different slopes of lines are observed (-0.011 and -0.030 cm^{-1} K^{-1}), which can be attributed to the variation of the soft mode frequency induced by the local spontaneous polarization (P_S) inside the PNRs [18–20]. Therefore, the various tendency of the Raman soft mode frequency with temperature agrees well with the PNRs in Pb-based ferroelectrics, in which unit cell volume deviates from linear thermal expansion at Burns temperature according to the XRD results in **Figure 3**. The current Raman study presents a novel method to characterize the relationship between the NTE and P_S of perovskite ferroelectric materials.
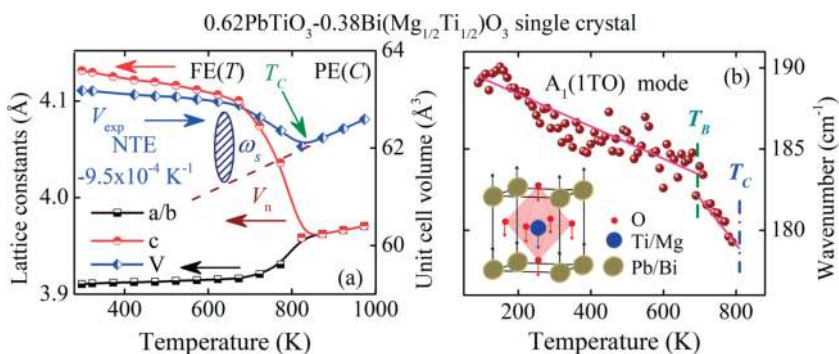

Figure 3. Temperature dependence of the lattice parameters and unit cell volume of the 0.62PT-0.38BMT crystal. FE(T) and PE(C) mean ferroelectric tetragonal phase and paraelectric cubic phase, respectively. The phonon frequency of soft mode as a function of temperature for 0.62PT-0.38BMT crystal. The solid lines indicate the different decrement of the soft mode with temperature (Figure reproduced with permission from [14]. Copyright 2016, Royal Society of Chemistry).

3.2. Tungsten bronze niobate ferroelectrics

Disordered ferroelectric systems are of great interest from the fundamental as well as applications points of view. The uniaxial relaxor ferroelectric SBN, which is of particular interest due to its well-known pyroelectric, electro-optic, and non-linear optical properties, has some potential applications such as holographic data storage, and generation of photorefractive solitons [21]. The aim of this part is to investigate the lattice vibration of the $Sr_xBa_{1-x}Nb_2O_6$ ceramics with different Sr/Ba ratios studied by Raman spectroscopy. The physical mechanism of the ferroelectric to paraelectric phase transition is found from the soft mode variation with the temperature. **Figure 4** shows Raman spectra of the SBN ceramics recorded at 150 K with different Sr compositions. The A_{1g} mode corresponding to a stretch type vibration of the NbO_6 octahedron decrease with increasing the Sr/Ba ratio. The Raman shift of the modes decreases from 643 and 612 cm^{-1} to 636 and 605 cm^{-1}, respectively. Another important feature observed in **Figure 4** is that the lowest modes (labeled with "*LM*") at about 42 cm^{-1} can be detected, which is inferred to the soft mode of the SBN ceramics. The soft mode is eigenvector approximated the ionic displacements occurring at a crystallographic phase transition in the ferroelectric material.

From the temperature dependence of the Raman spectra for all SBN ceramics in the temperature range from 150 to 750 K, the temperature evolution of the soft mode peak position is presented in **Figure 5**. The frequency of the soft modes decreases from 42 to 38 cm^{-1} with the Sr composition at 150 K. The phenomenon can be attributed to the A site substitution originated in the smaller ionic radius of Sr, as compared to Ba element. All frequency of the soft mode first decreases and then disappears in the SBN paraelectric phase. The T_C of the SBN ceramics shifts to lower temperature with increasing Sr composition. It can be well expressed by $T_C (x) = 566 - 371x$, where x is the Sr molar fraction. According to changes of the soft modes, it is clear that increasing Sr composition leads to the shrinking of T_C.
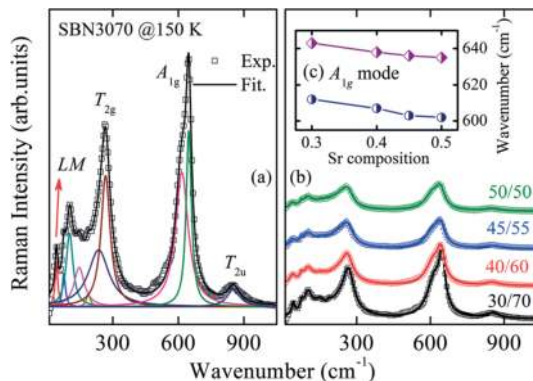

Figure 4. (a) Experimental Raman spectrum (dotted lines) and Lorentzian fitting results (solid lines) of the $Sr_{0.3}Ba_{0.7}Nb_2O_6$ ceramic at 150 K. The arrows indicate that the lowest phonon mode is located at about 40 cm^{-1} (labeled with "LM"). (b) Raman spectra of the SBN ceramics with different Sr composition recorded at 150 K. (c) The A_{1g} Raman-active phonon mode at about 636 and 605 cm^{-1} as a function of Sr composition.
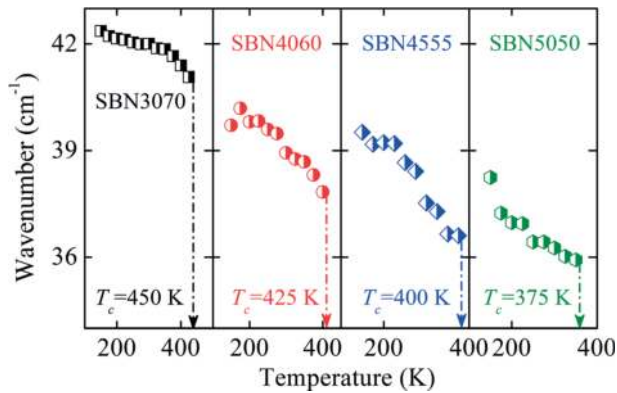
Figure 5. The soft mode frequency as a function of the temperature for the SBN ceramics. The dashed arrows show the temperature points where the soft mode vanishes.

3.3. Aurivillius-type bismuth layer-structured ferroelectrics

Recently, bismuth layer-structured ferroelectrics (BLSFs) have gained increasing attention for the promising applications of non-volatile random access memories (NvRAMs), optical switches and high-temperature piezoelectric devices, because of their relatively high T_c, low dielectric dissipation, and excellent hysteresis behavior [22–25]. Calcium bismuth niobate ($CaBi_2NbO_9$, CBN) is an Aurivillius layered material with the ultra-high T_c and relative higher thermal depoling temperature. The different properties induced by doping in BLSFs are always related to the structure distortions. The spectra of vibration modes in different frequencies could be sensitive to describe the structural distortion. As an example, **Figure 6** shows temperature-dependent Raman spectra of $CaBi_2Nb_{1.97}W_{0.03}O_9$ (W3) ceramic and the CBNW ceramics with different W compositions at 100 K. The results suggest that the peak center of ν5 deviated from the vertical dash line, and the color (in the web version) which represented the intensity of phonon mode faded with increasing temperature. This phenomenon means that the ν5 phonon mode was soften. However, there is no obvious change in the ν6 phonon mode upon heating, as compared to the behaviors of ν5. The similar Raman spectra with different W compositions also confirm that CBN doped with tungsten can keep single phase.

To further investigate the evolution of the ν5 and ν6 phonon modes, Raman spectra are well-fitted with multi-Lorentz oscillators. **Figure 7** shows Raman scattering results and well-fitted peaks with multi-Lorentz oscillators for all samples at 100, 300 and 800 K. The frequency, intensity and full width at half maximum of each phonon mode at different temperature can be derived from the fitting. The frequencies of the ν5 and ν6 phonon modes for W3 are presented in **Figure 8**. The shift of phonon modes can be explained by a simplified Klemens model [26].

From the fitting result according to the model, we can conclude that the change of the Raman phonon mode is dominated by the lattice expansion and thermal evolution. However, the intrinsic anharmonic coupling of phonons is quite weak for ν5. We can observe a slightly blue shift for ν6 phonon mode, while an opposite trend for ν5 in the whole temperature range. The
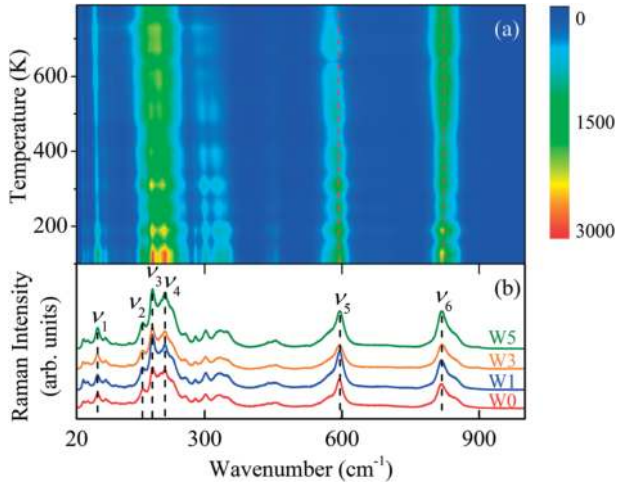
Figure 6. (a) Temperature-dependence of Raman spectra of CaBi$_2$Nb$_{1.97}$W$_{0.03}$O$_9$ (W3) ceramics from 100 to 800 K. (b) Raman scattering of CBNW ceramics with different W compositions at 100 K (Figure reproduced with permission from [22]. Copyright 2015, Elsevier).
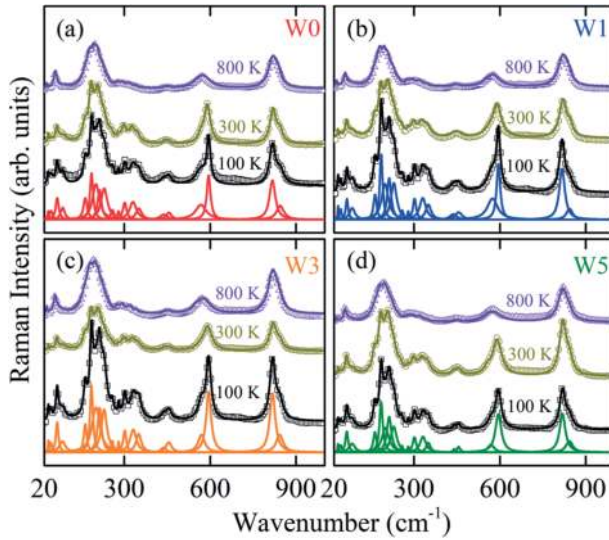

Figure 7. Experimental (dots) and the best fitting (solid lines) Raman spectra of CaBi$_2$Nb$_{2-x}$W$_x$O$_9$ ceramics with (a) 0, (b) 0.01, (c) 0.03, and (d) 0.05 at 100, 300 and 800 K, respectively (Figure reproduced with permission from [22]. Copyright 2015, Elsevier).

different changes between the phonon modes may be ascribed to the unusually strong and positive intrinsic anharmonicity instead of thermal evolution with increasing temperature. On the other hand, for all of the ceramics with increasing W composition, we found that the I(ν6)/I
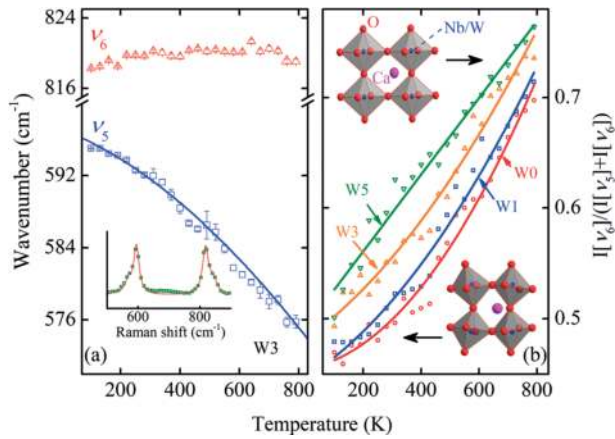
Figure 8. (a) Temperature-dependence of Raman phonon mode of ν5 (squares) and ν6 (trilateral). The inset shows the W3 Raman spectra at 100 K using Lorentz fitting. (b) the ratio of I(ν6)/I[(ν5) + I(ν6)] intensity with different W doping compositions (Figure reproduced with permission from [22]. Copyright 2015, Elsevier).

[(ν5) + I(ν6)] ratio increase with increasing temperature. The result is that the distortion degrees of perovskite (Nb, W)O_6 octahedra decrease with increasing temperature [27], and the BO_6 octahedra distortion predominates the structure distortion with Aurivillius niobate phase [28]. Thus, it can be concluded that the structure distortion in CBNW ceramics decreases with increasing W composition. The variation tendency is consistent with the XRD result in previous study. From the change of the Raman phonon modes with different temperature, we can see the parameter T_C generally decreases with the decrease of structure distortion degree [29, 30]. It was found that the relative peak intensity of I(ν6)/I[(ν5) + I(ν6)] ratio is sensitive for the distortion degree in ferroelectric materials. The Curie temperature of $CaBi_2Nb_{2-x}W_xO_9$ decreases with increasing composition from the Raman results, which is consistent with the results of dielectric permittivity experiments. The results indicate that the Raman spectrum is an effective tool for detecting structure distortion and phase transition of ferroelectric materials.

3.4. ABO$_3$ perovskite ceramics

In the past few decades, the complex Pb-based ABO_3 perovskite materials have attracted much attentions due to the excellent properties obtained in the compositions close to morphotropic phase boundary (MPB) [31]. The A-site substitution plays an important role in phase transition and more studies are requisite. In this part, the A-site substitution effect on the phase transition near MPB is investigated for PLZST ceramics. Transition temperature region and lattice dynamics are systematically discussed according to the temperature dependent Raman scattering spectroscopy. In addition, a new transient phase called the intermediate phase was found to exist between AFE and PE phase, which could be induced by defects through increasing temperature and doping of foreign ions.

Figure 9 depicts room-temperature Raman scattering results and well-fitted deconvolution peaks for all samples. A sharp increase of relative strength of E(TO2) mode could be observed
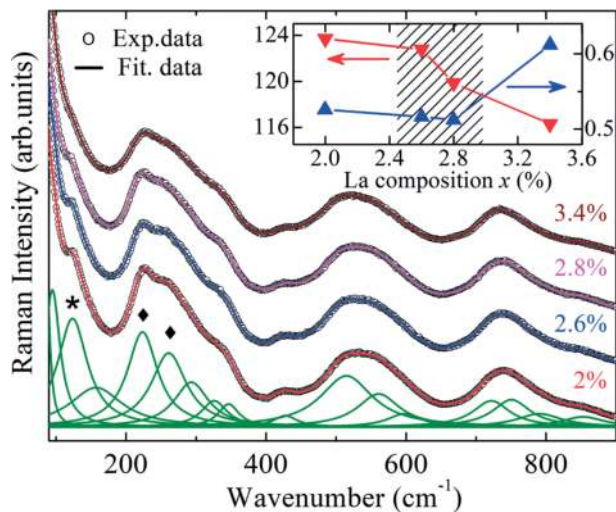
Figure 9. Raman scattering spectra of $Pb_{1-1.5x}La_xZr_{0.42}Sn_{0.4}Ti_{0.18}O_3$ ceramics with different La composition recorded at room temperature. The inset shows the frequency variation of A1(TO1) mode and relative strength of E(TO2) mode as a function of La composition (Figure reproduced with permission from [16]. Copyright 2013, American Institute of Physics).

at La composition of 2.8%. This indicates that PLZST3.4 ceramic is more likely to be tetragonal phase rather than the rhombohedral phase in the PLZST2 ceramic. The softing peak upon La composition is assigned as A1(TO1) symmetry, which stems from splitting of T_{1u} in cubic phase. The mode softs from 123.4 (PLZST2) to 116.3 cm^{-1} (PLZST3.4) with an incommensurate drop at La composition of 2.6%. The fact that both of two dramatic changes occur indicates the phase transition from rhombohedral to tetragonal structure for La composition between 2.6 and 2.8%.

To elucidate the thermal evolution of PLZST ceramics, temperature dependence of Raman spectra from 100 to 650 K are shown in **Figure 10**. We can see all of the Raman modes for the four PLZST ceramics have a blue shift with increasing temperature. Note that some of them disappear above 400 K during the cubic phase appearing. The results indicate that there is a structure transformation at about 400 K. Similar abnormal decrease in Raman intensity of PLZST ceramics has been detected by the spectra with increasing temperature.

To further investigate the phase transition mechanism, we plot temperature dependence of the wavenumber from the Raman modes in **Figure 11**. It can be found that some abrupt variations in the whole temperature range, which is easily divided into two phase transition regions. Note that there is a new intermediate phase at about 300 K for all of samples.

Figure 12 shows the phase diagram of PLZST ceramics according to the temperature dependence of Raman spectra. Three different structure phases can be found: AFE_O phase, intermediate phase, and PE_C phase. We can found that the PLZST ceramics have a transformation from AFEO to the intermediate phase with the composition of Ti exceeds 5.0% at room temperature. However, all of the ceramics remain cubic phase when the temperature upon 450 K. Note that the PLZST ceramics undergo successive phase transitions with increasing
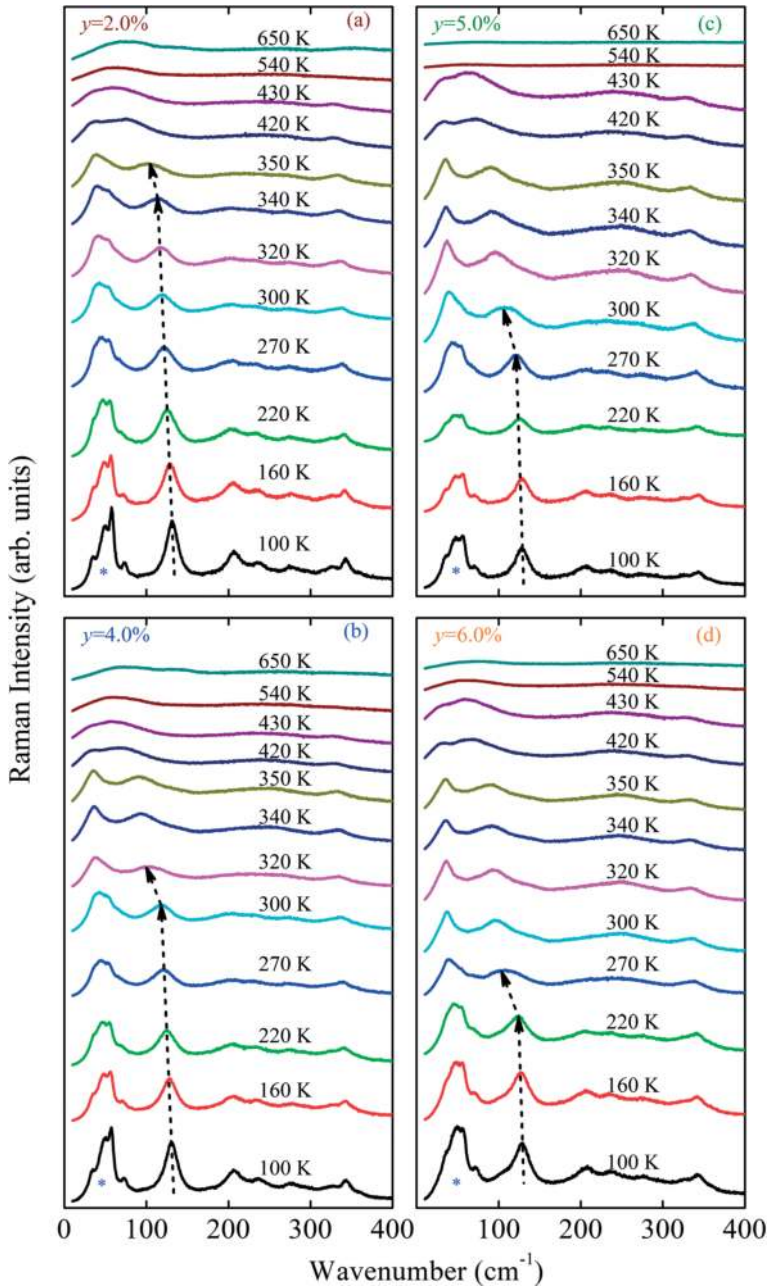
Figure 10. Temperature dependent Raman spectra for PLZST ceramics from 100 to 650 K. The symbol (*) represents the low wavenumber phonon modes (Figure reproduced with permission from [31]. Copyright 2016, Elsevier).
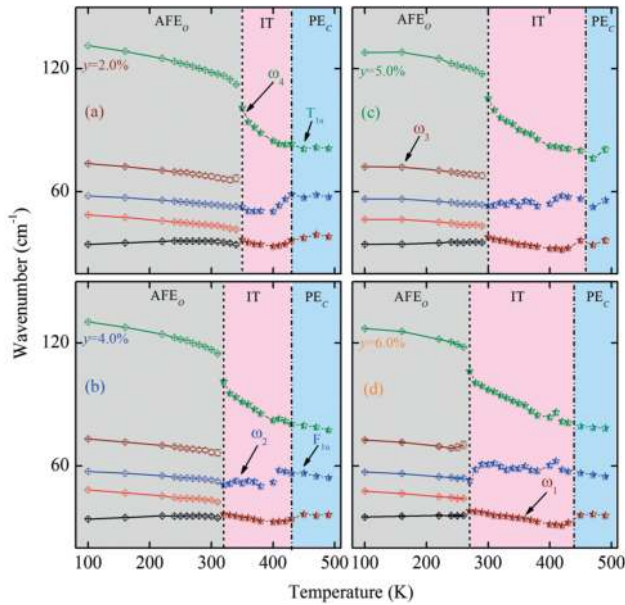
Figure 11. The variations of A1(TO1), AFD, E(TO1), and AHC modes as a function of temperature for PLZST ceramics with different Ti composition. Note that the dashed lines show the boundaries of two adjacent phase structures (Figure reproduced with permission from [31]. Copyright 2016, Elsevier).

temperature: from antiferroelectric phase at low temperature to intermediate phase and paraelectric cubic phase at high temperature. The Curie temperature for PLZST ceramics is lower than that of pure PZT materials because of some ions doping [32, 33]. Note that the intermediate boundaries in the phase diagram have a downward trend with Ti composition. However, the cubic phase boundaries almost remain the same temperature of about 400 K. The intermediate phase temperature ranges gradually become larger with increasing Ti compositions. The Curie temperature detected by Raman spectra are consist with the XRD and dielectric results, which suggests that the Raman spectrum is an effective tool to distinguish different phase structure in PZT ceramics with different temperature and doping level.

3.5. Multiferroics materials

$BiFeO_3$ (BFO) has been hailed as an important material for magnetoelectric devices due to its room-temperature multiferroic properties, in which the electric polarization is coupled to anti-ferromagnetic (AFM) order, allowing for manipulation of magnetism by applied electric fields and vice versa [34]. During the last several years, intriguing behavior was found in doped BFO compounds. In this part, we present Raman results on La and Ti codoped BFO ceramics to systematically study phase transitions induced by the chemical substitution and temperature.

Figure 13 demonstrates the spectra recorded at several characteristic temperatures and well-fitted deconvolution peaks at 80 K. The frequencies of the phonon modes shift to low energies and the intensity of all major peaks reduces as the temperature increases from 80 to 680 K. The modes in higher-frequency range become severely widening and merge into a broadening
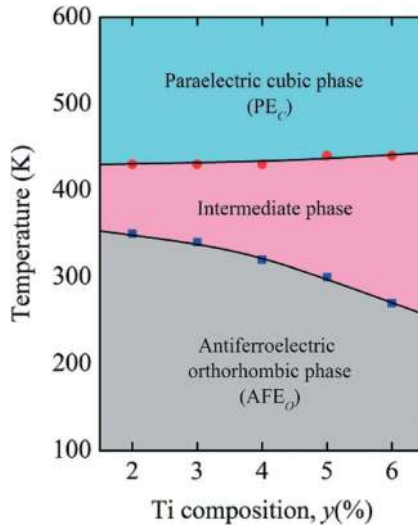
Figure 12. The phase diagram of PLZST ceramics based on the low wavenumber phonon mode variations with the temperature and Ti composition. The phase transformation regions of AFE_O, intermediate phase and PE_C characteristics can be clearly distinguished by the solid dots (Figure reproduced with permission from [31]. Copyright 2016, Elsevier).

peak. From the analysis of the mode position with the temperature, the anomalies in phonon modes suggest a strong magnon-phonon coupling of BLFTO in the present work.

Figure 14 shows composition dependence of the local structural transition temperature (T*) and Neel temperature (T_N). With the increase in the doping compositions of La and Ti, T* and T_N decrease from 580 to 540 K and from 645 to 630 K, respectively. According to La and Ti-codoped in BFO, an external pressure is induced due to size mismatch of host (Bi, Fe) and substitution (La, Ti) cations, which leads to the variation of tolerance factor and structural distortions. On the other hand, the strength of the antiferromagnetic superexchange interaction relies on the Fe-O-Fe angle. These structural effects weaken the magnetic exchange and decrease T_N. Thus, a complicated mechanism induced by the variation of bond length, bond angle, and the exchange interaction between adjacent magnetic moments could substantially contribute to the shrinking of Neel temperature. In summary, the Raman phonon modes have abnormal change around 140 and 205 K, which can be ascribed to the strong magnon-phonon coupling. The structural transition occurred at about 570 K can be detected by the Raman spectra, indicating that the Raman modes are sensitive to the structure changes and spin reorientation.

3.6. Lead-free ferroelectrics

Recently, KNN based lead-free materials were reported to offer comparable piezoelectric properties to that of PZT [35]. The $(K_{0.5}Na_{0.5})NbO_3$-$0.05LiNbO_3$-$yMnO_2$ (y = 0 and 1.0%) (KNN-LN-M) single crystals have been studied by the Raman spectra from the temperature 300–800 K. Moreover, the thermotropic phase boundaries are observed, indicating the existence of the mixed-phase region (i.e. PPT) between orthorhombic (O) and tetragonal (T) phases.
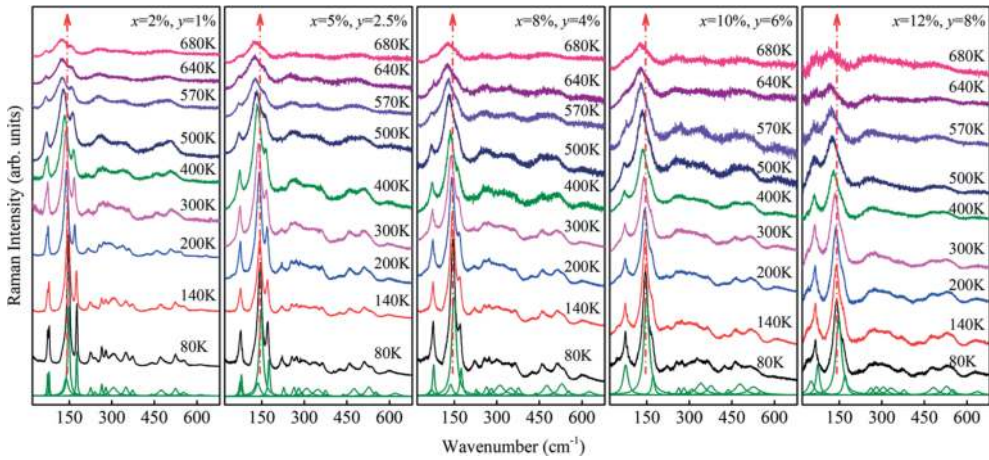
Figure 13. Temperature dependence of Raman scattering for the BLFTO ceramics collected in the temperature range from 80 to 680 K. As an example, Raman spectra recorded at 80 K, which were fitted with independent damped harmonic oscillators, have been indicated on the bottom (Figure reproduced with permission from [34]. Copyright 2014, American Institute of Physics).
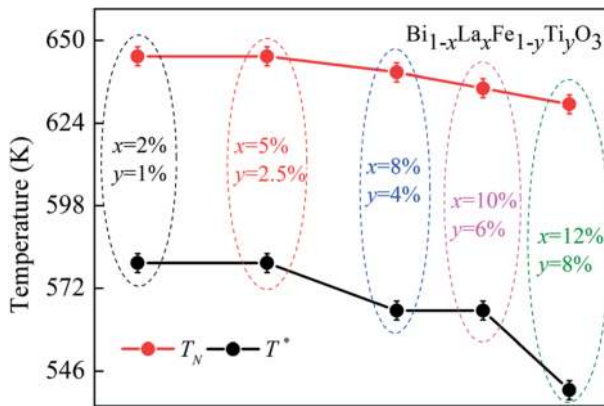

Figure 14. Composition dependence of phase transition temperature T* and Neel temperature TN for the BLFTO ceramics derived from temperature dependent Raman scattering (Figure reproduced with permission from [34]. Copyright 2014, American Institute of Physics).

Figure 15 depicts temperature dependence of Raman scattering for the KNN-LN and KNN-LN-1%MnO$_2$ crystals, respectively. The phase structure of KNN-LN based crystals transforms from O phase to T phase, then to cubic (C) phase with increasing temperature. The disorder in the O, T, and C phases can be characterized mainly by the Nb central ion allowed positions, and then the framework of the established eight-site model will be adopted [36]. In order to obtain a complete description of the dynamical properties through the successive phase transitions, it is useful to know the classification of the optical modes and their correlations between the various phases [37].

For a closer inspection, the peak positions of all modes in each phase are plotted in **Figure 16** against the temperature between 300 and 800 K. Frequency shifts and transformations of the modes are clear at the O-T and T-C boundaries. The trends within each phase consist primarily of mode softening with increasing temperature, exactly as expected to follow from the lattice thermal expansion. In the light of all the results, displacive and order–disorder mechanisms have to be associated in the description of the phase transitions. Thus, the successive phase transitions in KNN-LN based single crystals derive from competition between a soft phonon mode and a relaxation mode.

In order to obtain the phase fraction, we assume that one phase at thermal phase boundaries is a linear superposition of the spectra below and above phase boundaries. As shown in **Figure 17**, the fitting Raman spectra at 410–440 K in KNN-LN and KNN-LN-1%MnO$_2$, respectively, are displayed in comparison with the observed spectra at the same temperature. The fitting spectra are obtained from the linear superposition of the Raman spectra below and above phase boundaries. The coincidence of the experimental and the fitted Raman spectra are well for both samples, which strongly confirms the coexistence of the O and T phases at the thermal phase boundary from O to T phase. The mixed structure state at the thermal phase boundaries is due to sufficient competing mechanical and dipolar interactions between domains in multi-domain configurations [38]. In single domain case, the system undergoes a series of first-order ferroelectric transitions upon heating, sequentially adopting the O and T ferroelectric phases before reverting to the C parent phase.
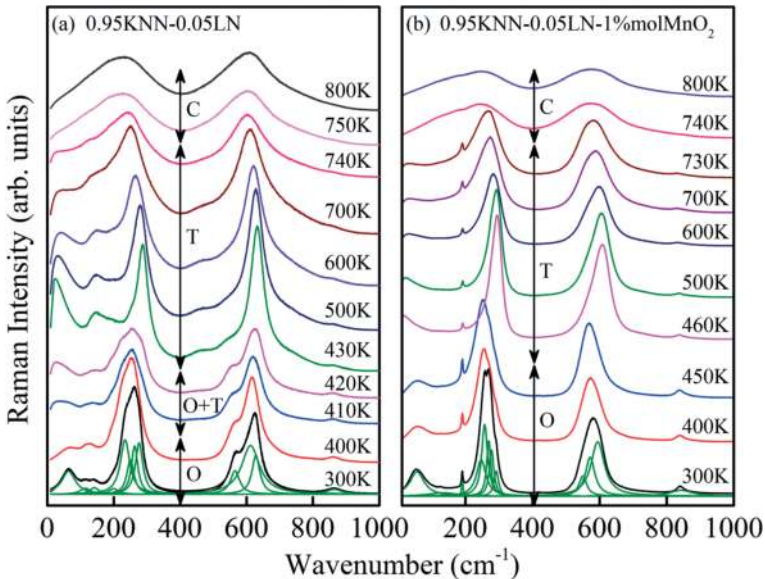

Figure 15. Temperature dependence of Raman scattering for the KNN-LN based single crystals collected in the temperature range from 300 to 800 K and Lorentzian-shaped deconvolution at the temperature of 300 K. The arrows are applied to separate different phase transition (Figure reproduced with permission from [35]. Copyright 2015, American Institute of Physics).
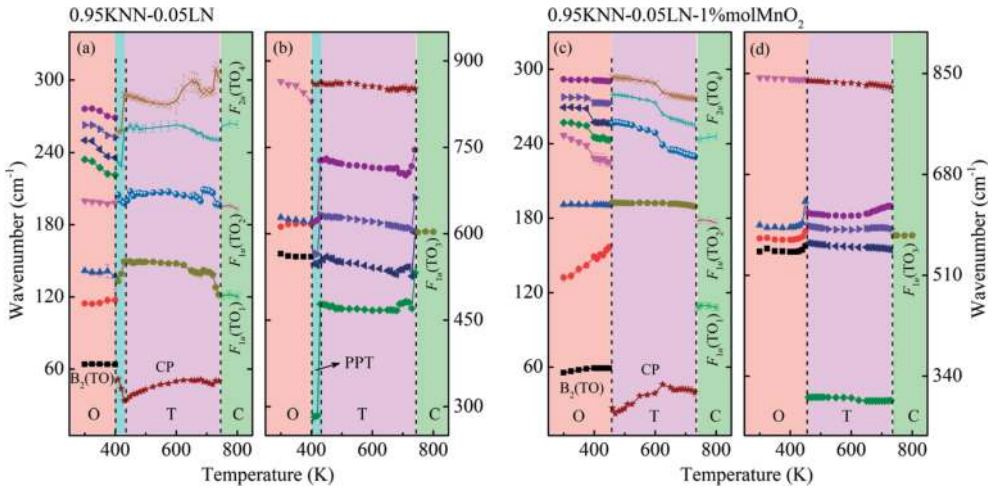
Figure 16. Temperature dependence of the phonon frequency from KNN-LN based crystals. (a) and (c): The low frequency range of 10–300 cm^{-1}, (b) and (d): The high frequency range of 400–900 cm^{-1}. Note that different shade regions indicate that the crystals are located in diverse phase (Figure reproduced with permission from [35]. Copyright 2015, American Institute of Physics).
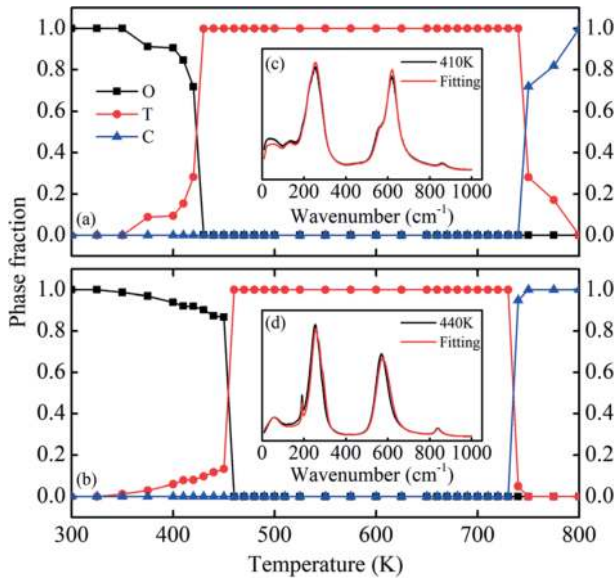

Figure 17. Phase fraction of (a) KNN-LN, and (b) KNN-LN-1%MnO$_2$ single crystals as a function of temperature. Note that (c) and (d) is the fitting Raman spectra at 410–440 K for KNN-LN and KNN-LN-1%MnO$_2$, respectively (Figure reproduced with permission from [35]. Copyright 2015, American Institute of Physics).

4. Conclusions and outlook

This chapter reports a systematic micro-Raman scattering study on A- and B-site doped lead-based, tungsten bronze niobate, Bi-layered, ABO_3 perovskites, multiferroics and lead-free ferroelectrics. The processing conditions, substitution, temperature-dependent Raman spectra and the structure–property correlations are discussed in the ceramics and single crystal forms of these materials. It can be concluded that the Raman spectra can provide us with a lot of important physical parameters for application in the future, such as spontaneous polarization, Curie temperature, structure distortion degree, mix-phase region and phase diagram and so on. The excellent agreement between the Raman, XRD or dielectric observations of merging of phase transition temperatures in all of the ferroelectric materials with different doping compositions suggested the powerful tool for detecting phase transition with solid state spectroscopy.

It should be emphasized that the domains in these ferroelectric materials and their related phenomena with different conditions, such as electric field, magnetic field and pressure have not been well investigated. The Raman spectra can be used to characterize the species of domain (including a/c domains, 90°/180° domains), critical sizes and domain wall in ferroelectrics. Thus, we can check the domain status by recording the high-resolution Raman response. Our next goal is to characterize the domain information in these ferroelectric ceramics and films and identify the factors which can affect the domain structure. We believe that our research results will be of great significance to the development of microelectronic physics in the future.

Acknowledgements

Author details

Kai Jiang, Liping Xu, Jinzhong Zhang, Zhigao Hu* and Junhao Chu

*Address all correspondence to: zghu@ee.ecnu.edu.cn

Technical Center for Multifunctional Magneto-Optical Spectroscopy (ECNU), Shanghai and Department of Electronic Engineering, East China Normal University, Shanghai, China

References

[1] Haertling GH. Ferroelectric ceramics: History and technology. Journal of the American Ceramic Society. 1999;**82**:797-818. DOI: 10.1111/j.1151-2916.1999.tb01840.x

[2] Dobal PS, Katiyar RS. Studies on ferroelectric perovskites and bi-layered compounds using micro-Raman spectroscopy. Journal of Raman Specroscopy. 2002;**33**:405-423. DOI: 10.1002/jrs.876

[3] Yang Y, Wang X, Sun C, Li L. Phase transition in $BaTiO_3$ nanotube arrays. Journal of Applied Physics. 2011;**109**:014109. DOI: 10.1063/1.3530614

[4] Pandey CS, Schreuer J, Burianek M, Muhlberg M. Relaxor behavior of ferroelectric $Ca_{0.22}Sr_{0.12}Ba_{0.66}Nb_2O_6$. Applied Physics Letters. 2013;**102**:022903. DOI: 10.1063/1.4775686

[5] Fan L, Chen J, Ren Y, Pan Z, Zhang L, Xing X. Unique piezoelectric properties of the monoclinic phase in $Pb(Zr,Ti)O_3$ ceramics: Large lattice strain and negligible domain switching. Physical Review Letters. 2016;**116**:027601. DOI: 10.1103/PhysRevLett.116.027601

[6] Schütz D, Deluca M, Krauss W, Feteira A, Jackson T, Reichmann K. Lone-pair-induced covalency as the cause of temperature- and field-induced instabilities in bismuth sodium Titanate. Advanced Functional Materials. 2012;**22**:2285-2294. DOI: 10.1002/adfm.201102758

[7] Grinberg I, Cooper VR, Rappe AM. Relationship between local structure and phase transitions of a disordered solid solution. Nature. 2002;**419**:909-911. DOI: 10.1038/nature01115

[8] Sun Y, Welch GC, Leong WL, Takacs CJ, Bazan GC, Heeger AJ. Solution-processed small-molecule solar cells with 6.7% efficiency. Nature Materials. 2012;**11**:44-48. DOI: 10.1038/nmat3160

[9] Dupe B, Prosandeev S, Geneste G, Dkhil B, Bellaiche L. $BiFeO_3$ films under tensile epitaxial strain from first principles. Physical Review Letters. 2011;**106**:237601. DOI: 10.1103/PhysRev Lett.106.237601

[10] Khalyavin DD, Salak AN, Vyshatko NP, Lopes AB, Olekhnovich NM, Pushkarev AV, Maroz II, Radyush YV. Crystal structure of metastable perovskite $bi(Mg_{1/2}Ti_{1/2})O_3$: Bi-based structural analogue of antiferroelectric $PbZrO_3$. Chemistry of Materials. 2006;**18**:5104-5110. DOI: 10.1021/cm061129w

[11] Rusakov DA, Abakumov AM, Yamaura K, Belik AA, Van Tendeloo G, Takayama-Muromachi E. Structural evolution of the $BiFeO_3-LaFeO_3$ system. Chemistry of Materials. 2010;**23**:285-292. DOI: 10.1021/cm1030975

[12] Damodaran AR, Liang C-W, He Q, Peng C-Y, Chang L, Chu Y-H, Martin LW. Nanoscale structure and mechanism for enhanced electromechanical response of highly strained $BiFeO_3$ thin films. Advanced Materials. 2011;**23**:3170-3175. DOI: 10.1002/adma.201101164

[13] Liu J, Chen X, Xu G, Yang D, Tian Y, Zhu X. Novel high-temperature ferroelectric single crystals $0.38Bi(Mg_{1/2}Ti_{1/2})O_3$-$0.62PbTiO_3$ with good and temperature-stable piezoelectric properties. CrystEngComm. 2015;**17**:5605-5608. DOI: 10.1039/C5CE01114K

[14] Jiang K, Zhang P, Zhang J, Xu G, Li W, Hu Z, Chu J. Relationship between negative thermal expansion and lattice dynamics in a tetragonal $PbTiO_3$-bi$(Mg_{1/2}Ti_{1/2})O_3$ perovskite single crystal. RSC Advances. 2016;**6**:3159-3164. DOI: 10.1039/C5RA24408K

[15] Liang P, Kai J, Jinzhong Z, Zhigao H, Genshui W, Xianlin D, Junhao C. Temperature-dependent phonon Raman scattering and spectroscopic ellipsometry of pure and Ca-doped $Sr_xBa_{1-x}Nb_2O_6$ ferroelectric ceramics across the phase transition region. Journal of Physics D: Applied Physics. 2016;**49**:035307. DOI: 10.1088/0022-3727/49/3/035307

[16] Chen X, Hu ZG, Duan ZH, Chen XF, Wang GS, Dong XL, Chu JH. Effects from A-site substitution on morphotropic phase boundary and phonon modes of $(Pb_{1-1.5x}La_x)(Zr_{0.42}Sn_{0.40}Ti_{0.18})O_3$ ceramics by temperature dependent Raman spectroscopy. Journal of Applied Physics. 2013;**114**:043507. DOI: 10.1063/1.4816093

[17] Zhang J, Tong W-Y, Zhu J, Xu J, Duan Z, Xu L, Hu Z, Duan C-G, Meng X, Zhu Z, Chu J. Temperature-dependent lattice dynamics and electronic transitions in 0.93Pb$(Zn_{1/3}Nb_{2/3})$ O_3-0.07PbTiO$_3$ single crystals: Experiment and theory. Physical Review B. 2015;**91**:085201. DOI: 10.1103/PhysRevB.91.085201

[18] Chen J, Hu L, Deng J, Xing X. Negative thermal expansion in functional materials: Controllable thermal expansion by chemical modifications. Chemical Society Reviews. 2015;**44**:3522-3567. DOI: 10.1039/C4CS00461B

[19] Zhang Q, Li Z, Xu Z. Phase transition in (1-x)Bi$(Mg_{1/2}Ti_{1/2})O_3$-xPbTiO$_3$ ceramics. Materials Letters. 2011;**65**:3143-3145. DOI: 10.1016/j.matlet.2011.06.078

[20] Bokov AA, Ye ZG. Recent progress in relaxor ferroelectrics with perovskite structure. Journal of Materials Science. 2006;**41**:31-52. DOI: 10.1007/s10853-005-5915-7

[21] Dec J, Kleemann W, Miga S, Shvartsman VV, Łukasiewicz T, Świrkowicz M. Aging, rejuvenation, and memory effects in the domain state of $Sr_{0.75}Ba_{0.25}Nb_2O_6$. Phase Transitions. 2007;**80**:131-140. DOI: 10.1080/01411590701315492

[22] Shi K, Peng L, Li M, Zhou Z, Jiang K, Zhang J, Hu Z, Dong X, Chu J. Structural distortion, phonon behavior and electronic transition of Aurivillius layered ferroelectric $CaBi_2Nb_{2-x}W_xO_9$ ceramics. Journal of Alloys and Compounds. 2015;**653**:168-174. DOI: 10.1016/j.jallcom.2015.09.037

[23] Kleemann W, Dec J, Shvartsman VV, Kutnjak Z, Braun T. Two-dimensional ising model criticality in a three-dimensional uniaxial relaxor ferroelectric with frozen polar nano-regions. Physical Review Letters. 2006;**97**:065702. DOI: 10.1103/PhysRevLett.97.065702

[24] Zhang J, Wang G, Gao F, Mao C, Cao F, Dong X. Influence of Sr/Ba ratio on the dielectric, ferroelectric and pyroelectric properties of strontium barium niobate ceramics. Ceramics International. 2013;**39**:1971-1976. DOI: 10.1016/j.ceramint.2012.08.048

[25] Kitaev YE, Aroyo MI, Perez-Mato JM. Site symmetry approach to phase transitions in perovskite-related ferroelectric compounds. Physical Review B. 2007;**75**:064110. DOI: 10.1103/PhysRevB.75.064110

[26] Balkanski M, Wallis RF, Haro E. Anharmonic effects in light scattering due to optical phonons in silicon. Physical Review B. 1983;**28**:1928-1934. DOI: 10.1103/PhysRevB.28.1928

[27] Shimakawa Y, Imai H, Kimura H, Kimura S, Kubo Y, Nishibori E, Takata M, Sakata M, Kato K, Hiroi Z. Orbital hybridization and covalency in paraelectric and ferroelectric $SrBi_2Nb_2O_9$. Physical Review B. 2002;**66**:144110. DOI: 10.1103/PhysRevB.66.144110

[28] Shimakawa Y, Kubo Y, Tauchi Y, Kamiyama T, Asano H, Izumi F. Structural distortion and ferroelectric properties of $SrBi_2(Ta_{1-x}Nb_x)_2O_9$. Applied Physics Letters. 2000;**77**:2749-2751. DOI: 10.1063/1.1319509

[29] Sun L, Chu J, Feng C, Chen L. Analysis of relaxor mechanism and structural distortion for $SrBi_{1.6}Nd_{0.4}Nb_2O_9$ bismuth-layer-structured ceramics. Applied Physics Letters. 2007;**91**: 242902. DOI: 10.1063/1.2824383

[30] Blake SM, Falconer MJ, McCreedy M, Lightfoot P. Cation disorder in ferroelectric Aurivillius phases of the type $Bi_2ANb_2O_9$(A=Ba, Sr, Ca). Journal of Materials Chemistry. 1997;**7**:1609-1613. DOI: 10.1039/A608059F

[31] Ding X, Guo S, Hu Z, Chen X, Wang G, Dong X, Chu J. The intermediate phase and low wavenumber phonon modes in antiferroelectric $(Pb_{0.97}La_{0.02})(Zr_{0.60}Sn_{0.40-y}Ti_y)O_3$ ceramics discovered from temperature dependent Raman spectra. Journal of Alloys and Compounds. 2016;**667**:310-316. DOI: 10.1016/j.jallcom.2016.01.188

[32] Buixaderas E, Gregora I, Kamba S, Petzelt J, Kosec M. Raman spectroscopy and effective dielectric function in PLZTx/40/60. Journal of Physics: Condensed Matter. 2008;**20**:345229. DOI: 10.1088/0953-8984/20/34/345229

[33] Jankowska-Sumara I. Antiferroelectric phase transitions in single crystals $PbZrO_3$:Sn revisited. Phase Transitions. 2014;**87**:685-728. DOI: 10.1080/01411594.2014.900554

[34] Xu LP, Zhang LL, Zhang XL, Zhang JZ, Hu ZG, Yu J, Chu JH. Phase transformations in multiferroic $Bi_{1-x}La_xFe_{1-y}Ti_yO_3$ ceramics probed by temperature dependent Raman scattering. Journal of Applied Physics. 2014;**116**:164103. DOI: 10.1063/1.4900439

[35] Xu LP, Jiang K, Zhang JZ, Xu GS, Hu ZG, Chu JH. Phase transitions and thermotropic phase boundaries in MnO_2-doped $(K_{0.5}Na_{0.5})NbO_3$-0.05$LiNbO_3$ single crystals: Raman scattering evidence at elevated temperatures. Applied Physics Letters. 2015;**106**:122901. DOI: 10.1063/1.4916226

[36] Pruzan P, Gourdain D, Chervin JC. Vibrational dynamics and phase diagram of $KNbO_3$ up to 30 GPa and from 20 to ~500 K. Phase Transitions. 2007;**80**:1103-1130. DOI: 10.1080/01411590701473176

[37] Fontana MD, Metrat G, Servoin JL, Gervais F. Infrared spectroscopy in $KNbO_3$ through the successive ferroelectric phase transitions. Journal of Physics C: Solid State Physics. 1984;**17**:483. DOI: 10.1088/0022-3719/17/3/020

[38] Lummen TTA, Gu Y, Wang J, Lei S, Xue F, Kumar A, Barnes AT, Barnes E, Denev S, Belianinov A, Holt M, Morozovska AN, Kalinin SV, Chen L-Q, Gopalan V. Thermotropic phase boundaries in classic ferroelectrics. Nature Communications. 2014;**5**:3172. DOI: 10.1038/ncomms4172